Nanomechanical Properties of TiO_2 Granular Thin Films

Houman Yaghoubi,[†,‡] Nima Taghavinia,[*,§,∥] Eskandar Keshavarz Alamdari,[†,⊥] and Alex A. Volinsky[‡]

New Materials Department, Materials and Energy Research Center (MERC), P.O. Box 14155-4777, Tehran, Iran, Physics Department, Sharif University of Technology, Tehran 14588, Iran, Institute for Nanoscience and Nanotechnology, Sharif University of Technology, Tehran 14588, Iran, Department of Mining and Metallurgical Engineering, Amirkabir University of Technology, 424 Hafez Avenue, P.O. Box 15875-4413, Tehran, Iran, and Department of Mechanical Engineering, University of South Florida, Tampa, Florida 33620

ABSTRACT Post-deposition annealing effects on nanomechanical properties of granular TiO_2 films on soda-lime glass substrates were studied. In particular, the effects of Na diffusion on the films' mechanical properties were examined. TiO_2 photocatalyst films, 330 nm thick, were prepared by dip-coating using a TiO_2 sol, and were annealed between 100 °C and 500 °C. Film's morphology, physical and nanomechanical properties were characterized by atomic force microscopy, X-ray photoelectron spectroscopy, X-ray diffraction, differential thermo-gravimetric analysis, and nanoindentation. Contrary to expectations, the maximum film hardness was achieved for 300°C annealing, with a value of 0.69 ± 0.05 GPa. Higher annealing temperatures resulted in inferior mechanical properties. No pile-up or sink-in effects were observed with minimal creep for the 300 °C annealed sample. Considerable decrease in the amount of chemisorbed water was found with increasing annealing temperature, causing gel films densification, explaining the increasing trend of hardness with annealing temperature between 100 °C and 300 °C. DTA/TGA results also confirmed the weight loss and the endothermic reaction due to desorption of chemisorbed water. Decrease in hardness above 300 °C annealing is attributed to thermal diffusion of Na ions from the glass substrate, confirmed by nanoindentation tests on TiO_2 films deposited on fused quartz, which did not exhibit hardness decrease after 300 °C annealing.

KEYWORDS: TiO_2 • self-cleaning • photocatalyst • nanoindentation • Berkovich indenter

1. INTRODUCTION

TiO_2 films are widely used in applications such as self-cleaning coatings (1−5), dye-sensitized solar cells (6−14), water detoxification and purification (15−19), air treatment (3, 5, 20−23), and food storage (24, 25). TiO_2 is a favored photocatalyst compared to other materials because of good photoactivity, photo and chemical stability, non-toxicity, low cost, and availability (26). Good mechanical performance of TiO_2 self-cleaning coatings is essential because they are usually exposed to severe service conditions. TiO_2 self-cleaning coatings are usually applied by dip or spray coating of a nanoparticle sol on a surface (27), with a typical thickness of a few hundred nanometers. TiO_2 films are formed by an evaporation-induced condensation process, which results in a gel film containing a few weight percent water (27, 28). Annealing of films leads to enhanced crystallinity, as well as removal of volatile species from the film. Better crystallinity is crucial in many photocatalytic applications. High-temperature annealing is also known to enhance films mechanical properties, mainly due to sintering of granular films, as well as chemical attachment to the substrate. For TiO_2 films on glass, 500 °C is typically considered a maximum annealing temperature because of the anatase to rutile phase transition, as well as substrate softening effects (1, 29−32). Therefore, TiO_2 sol−gel films are frequently annealed at about 500 °C to enhance both crystallinity and mechanical properties.

For TiO_2 films deposited on glass, there is an extra issue of Na diffusion from the substrate, which affects the films properties. Although it was known from the early years of research on photocatalysts that Na diffusion from substrate has an adverse effect on TiO_2 photocatalytic properties, there are few quantitative reported studies. Nam and coworkers studied the effect of Na diffusion on photocatalytic properties of TiO_2 sol−gel films (33) and found that photocatalytic activity is increased with temperature due to the constructive effect of Na on the anatase crystal formation. They also noted that sodium ions cannot be regarded as recombination centers. To the best of our knowledge, there are no systematic studies that demonstrate the influence of Na diffusion on mechanical properties of TiO_2 films. In this study, we found that 300 °C is an optimal annealing temperature for mechanical, as well as photocatalytic properties of TiO_2 films on glass. This could be a practically important fact, as 300 °C heat treatment is applicable in on-site self cleaning glass applications.

* Corresponding author. Tel. & Fax: +98-(21)-66164532. E-mail: taghavinia@sharif.edu.

Received for review May 21, 2010 and accepted August 6, 2010

† Materials and Energy Research Center.

‡ University of South Florida.

§ Physics Department, Sharif University of Technology.

∥ Institute for Nanoscience and Nanotechnology, Sharif University of Technology.

⊥ Amirkabir University of Technology.

DOI: 10.1021/am100455q

This study of mechanical properties is based on nanoindentation tests of granular TiO_2 films. To the best of our knowledge, the behavior of granular porous TiO_2 films under indentation has not been carefully studied so far. There are few reports on the nanomechanical properties of TiO_2 thin films (34, 35). Nanoindentation provides reliable data for thin films and has been successfully employed for a number of films including carbon nitride and Cu (36), Sn and Ni−Sn (37), and nanocrystalline Ni (38). For thin coatings on substrates conventional techniques such as tensile test are not applicable. Depth-sensing indentation is an alternative and a relatively new approach that provides more precise information, as it utilizes extremely low loads, where indentation-induced cracking can be largely avoided (39−41). Usefulness of instrumented nanoindentation has been well demonstrated (42−45). Efforts including presenting theoretical models have been performed to investigate interfacial reactions happening under indentation (46).

2. EXPERIMENTAL SECTION

2.1. Materials and Synthesis. Glass plates (35 mm ×25 mm ×1.5 mm) were used as substrates. First the substrates were washed with detergent and deionized (DI) water and further cleaned with extra-pure acetone (Scharlau Chemie S.A., 99.5% purity). Subsequently, they were rinsed with DI water and dried. Glass plates were then placed in an electric furnace at 400 °C for 30 min in order to remove residual organic contaminants and enhance wettability.

A peroxotitanium complex solution was prepared by mixing titaniumtetraisopropoxide (TTIP) (Merck, purity ≥99.5%), H_2O_2 (Merck, 30%) and H_2O, with volume proportions of 12:90:200, respectively. Solution pH was then raised to 7.0. The resulting solution was refluxed at 90 °C for 10 h to obtain crystalline anatase sol (47). Gel films were formed on the substrates from the 1 wt % TiO_2 sol by dip coating with withdrawal speed of 9.2 mm/s. For all the samples, a pre-coat of the peroxotitanium complex solution (the sol before reflux) was applied to enhance the adhesion. Subsequent layers of crystalline TiO_2 were deposited by dip coating 4 times. The samples were dried after each dip at 100°C for 15 min. Finally, the samples were annealed in the range between 100 and 500 °C for 1 h in air using an electric furnace (Azar Furnaces M2L 1200). The thickness of TiO_2 films was estimated to be 330±5 nm by simulating optical transmittance spectra, as reported earlier (47−50).

2.2. Characterization. Mechanical properties of the films were characterized using a TriboScope nanomechanical test instrument (Hysitron Inc.) with a two-dimensional transducer in conjunction with an Atomic Force Microscope (NanoScope III, Digital Instruments). A Berkovich diamond indenter with 135 nm tip radius was used for all measurements. Tip area function was calibrated by using fused silica sample in the appropriate depth range.

Indentation time was set to 30 s for loading and 30 s for unloading steps. To account for thermal drift, we introduced a 10 s hold time between loading and unloading cycles. The peak load was determined such that an indentation depth of ∼30% of the TiO_2 film thickness was achieved. It has been demonstrated that an indentation depth of less than 30% of the film thickness helps to avoid substrate contributions to film's mechanical properties (37, 51, 52). Three indentations were made at constant maximum load of 125 μN and then the mechanical properties values were averaged to obtain the mean value and standard deviation. The results presented in this paper have the standard deviation of less than 10%. Scratch tests were performed using the same Berkovich tip with 60 s scratching time and 4 μm scratching distance. The normal force was kept constant at 40 μN.

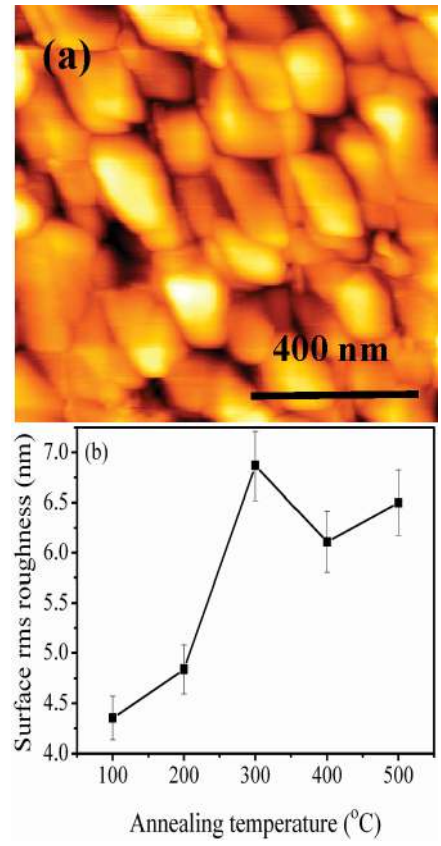

FIGURE 1. (a) Surface morphology of TiO_2 film annealed at 100 °C. (b) Rms surface roughness of films vs annealing temperature.

Atomic force microscopy (AFM) was carried out using a Park Scientific Instruments microscope (AUTOPROBE CP). X-ray photoelectron spectroscopy (XPS) used a monochromatized Al K_α X-ray source and a hemispherical energy analyzer (Spec model EA10+). The peaks were referenced to the C 1s peak (E_B = 285.0 eV). X-ray diffraction (XRD) measurements were performed using a Unisantis diffractometer model XMD-300 with Cu K_α. radiation (1.54 Å). Differential thermal analysis/thermo-gravimetric analysis (DTA/TGA) measurements were performed using STA 1640 thermal analyzer (Polymer Laboratories) in air with a heating rate of 5 °C/min. Samples were heated up to 600 °C. Contact angle (CA) measurements were performed using 2 μL water droplets and a CCD camera connected to a computer (Dataphysics, OCA15plus).

Photocatalytic activity was evaluated by monitoring the decreasing trend of CA as a result of the photo-decomposition of a stearic acid thin layer on the films (one droplet of stearic acid spin coated on the TiO_2 surface at 2000 rpm for 30 s). Samples were irradiated from the top using an ultraviolet (UV) lamp (Philips TUV 4 W, main spectral peak: 254 nm) at 11 mW/cm^2.

3. RESULTS

3.1. Films Morphology. Figure 1a shows the AFM image of films annealed at 100 °C. The morphology for other samples is similar. The grain size corresponds to the size of TiO_2 nanoparticles in the sol, which have piled up to form the granular film. TiO_2 nanoparticles independently observed using transmission electron microscopy (TEM) are ellipsoidal in shape with mean short and long axis of 15 and 54 nm (53). High porosity of films implies a large surface

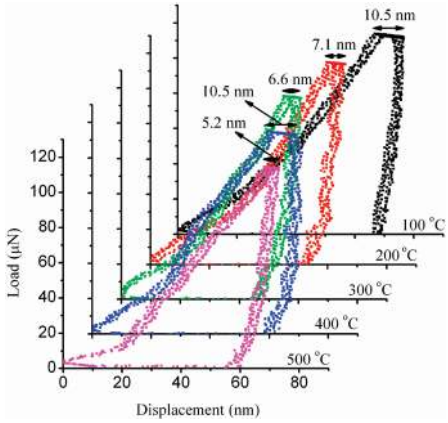

FIGURE 2. Load−displacement curves and displacement during hold time (creep) for the TiO_2 films annealed between 100 and 500°C.

area and enhances photocatalytic activity. Mechanical properties are also influenced by the films porosity, making the hardness and elastic modulus different from the bulk values. Figure 1b displays the surface roughness values obtained from the analysis of AFM images. Surface roughness increased up to 6.75 nm at 300 °C annealing temperature and then remained fairly constant with higher annealing temperature.

3.2. Nanomechanical Testing: Nanoindentation. Nanoindentation tests were performed to measure hardness, creep and modulus of elasticity of the films. Load−displacement data were analyzed to obtain hardness and indentation modulus using a power-law fit following the method of Oliver and Pharr (54). Young's modulus is a measure of the resistance to small changes in separation of adjacent atoms related to interatomic bonding forces and its magnitude depends on the slope of the force-displacement curv (55).

Figure 2 shows load−displacement curves for the TiO_2 films annealed between 100 °C and 500 °C. The samples show a similar trend where the maximum displacement decreases with increased annealing temperature from 100 to 300 °C. From 300 to 400 °C, the displacement increases and remains fairly constant up to 500 °C annealing temperature. Figure 2 also illustrates that the loading curves for all samples are continuous, suggesting that no cracking occurred during loading. For all TiO_2 film samples displacement increases during the hold at maximum load due to creep. The creep during 10 s hold time for samples annealed between 100 and 500 °C was about 10.5, 7.1, 6.6, 10.5, and 5.2 nm, respectively. Moreover, in the indentation of the TiO_2 films, no pull-off portion of the unloading curve was observed, implying that there was negligible adhesion between the Berkovich tip and the films. The curves exhibit very low scatter and the data are quite repeatable.

Reduced modulus of elasticity and hardness calculated from the load−displacement curves are shown in Figure 3a. Increasing annealing temperature from 100 to 300 °C resulted in hardness increase from 0.42 ± 0.05 GPa to 0.69 ± 0.05 GPa. Further increase in temperature up to 500 °C resulted in a decrease of both the hardness and the elastic modulus. The films annealed at 300°C exhibited hardness

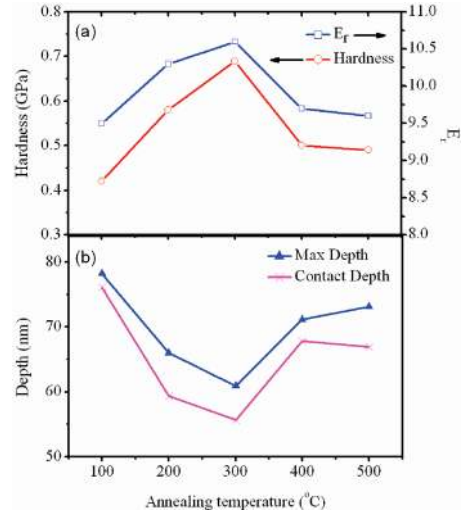

FIGURE 3. Variations in (a) hardness and reduced modulus, (b) contact depth and maximum penetration depth as functions of annealing temperature.

of about 1.4 times that of the films annealed at 500 °C. The variation of modulus with annealing temperature is similar to hardness and shows a maximum at 300°C with a value of 10.6 GPa. Figure 3b shows a variation of the contact depth and the maximum penetration depth vs. temperature. Both show a minimum at 300 °C, which corresponds to the maximum film hardness value.

Indentation behavior of TiO_2 films can be found from an experimentally measured parameter, which is the ratio of the final indentation depth, h_f, to the depth of indentation at the peak load, h_{max} (56). The h_f/h_{max} ratio can be easily extracted from the unloading curves and is always between 0 and 1. The lower limit corresponds to fully elastic deformation, while the upper limit relates to plastic behavior. The ratio for TiO_2 films is ~0.86−0.89, which implies plastic deformation of the films at the 125 μN load when indentation curves give almost film-only properties.

One of the sources of error in the estimation of hardness and modulus values is the appearance of pile-up and/or sink-in effects at the edges of the residual indents. These effects cause inaccuracy in the estimation of contact area. Valuable discussions have been made to express the effect of the pile-up and sink-in on hardness (36). Pile-up can be evaluated using the topographic profiles and AFM images of the indentation marks on the sample. AFM images and the corresponding section analysis plots clearly showed that there is no pile-up or sink-in at the edges of the residual indents.

The scratch resistance has also been calculated, which shows significant increasing trend up to 300 °C annealing temperature with no noticeable improvement above that temperature. This is similar to the hardness and elastic modulus trends.

3.3. Chemical Composition and Crystallinity. Analyses were carried out using information from XPS, DTA/TGA, and XRD. The survey XPS spectrum of TiO_2 films annealed between 100 °C and 500 °C (Figure 4) showed Ti, O, C, and Na elements on the film's surface. C resulted from adsorbed pollutants and adventitious hydrocarbon mol-

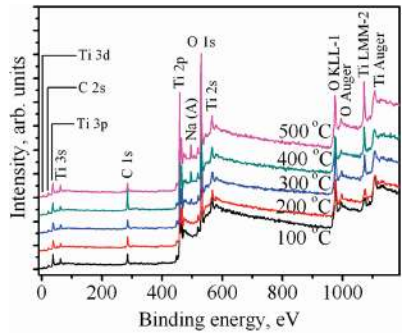

FIGURE 4. XPS survey spectra for TiO_2 thin films annealed between 100 and 500 °C.

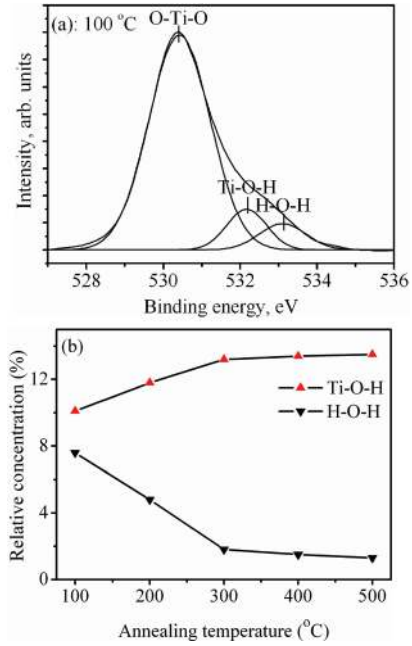

FIGURE 5. (a) XPS spectrum of the O 1s region for 100 °C annealed sample and (b) atomic percentage of O in H−O−H and Ti−O−H as a function of annealing temperature.

ecules. Appearance of Na is caused by diffusion of mobile Na ions from the soda-lime glass substrate observed for the films annealed at $T \geq 300$ °C. It is evident that the atomic percent of Na has increased noticeably as a function of annealing temperature.

Figure 5 shows XPS spectrum of the O 1s region for 100 °C annealed samples as a typical and the relative concentration of H−O−H and Ti−O−H groups as a function of annealing temperature. Three chemical compositions can be considered as the sources of O peak in the XPS spectra: (a) Ti−O−Ti bonds of TiO_2, (b) Ti−O−H bonds on the surface of TiO_2, and (c) H−O−H bonds of the chemisorbed H_2O molecules. The XPS spectra were decomposed into three corresponding peaks, where the main peak is attributed to Ti−O−Ti. On the basis of the intensity of the decomposed peaks, the relative concentration of Ti−O−Ti, Ti−O−H, and H−O−H groups has been estimated and listed in Table 1. A relatively large amount of chemisorbed water is present in the sol−gel coating, as shown for the 100 °C annealed sample. It is observed that the relative concentration of the chemisorbed water has dropped from 7.6 % to 1.3 % for the

Table 1. Fitting Results for the High-Resolution Spectra of the Ti 2p Region; Rel. (%) Represents the Relative Contribution of Each Peak

		Rel. (%)	
binding energy (eV)	530.42	532.18	533.1
T (°C)	O1s, Ti−O−Ti	O1s, Ti−O−H	O1s, H−O−H
100	82.3	10.1	7.6
200	83.4	11.8	4.8
300	85.0	13.2	1.8
400	85.1	13.4	1.5
500	85.2	13.5	1.3

films annealed between 100 °C and 500 °C, with the major change occurring below 300 °C. The decrease in the chemisorbed water concentration is accompanied with a slight increase in Ti−O−H and Ti−O−Ti proportions. The increase in Ti−O−H may be due to disappearing H_2O molecules, which expose the hydrolyzed surface behind. It has also been reported that annealing of single-crystalline TiO_2 induces surface defects that produce favored sites for the OH groups' adsorption (57−60). Water desorption due to annealing is known to initiate the condensation reaction in the sol−gel process of TiO_2 formation (61, 62).

TGA/DTA curves of the dip coated samples are shown in Figure 6. TGA graph represents a typical stage of weight loss below 100 °C due to the evaporation of residual water. It is followed by another rapid weight loss at temperatures between 200 and 300 °C. There is also a DTA peak of an endothermic reaction at 213 °C. This can be generally attributed to the chemisorbed water desorption, also evidenced by XPS results. Overall, the TGA results show a loss of 20% up to 350 °C annealing. Sample weight remains almost unchanged after this temperature.

DTA/TGA results are in agreement with other reports available in the literature. Egashira et al. carefully studied the adsorbed state of water on TiO_2 (anatase) with temperature programmed desorption (TPD) and demonstrated that two H_2O desorption peaks can be observed, with the maxima at 69−127 °C and 191−256 °C, with an enthalpy of the endothermic reaction for the latter peak of about 55−69 KJ mol^{-1} (63). Our results show the desorption peak at 213 °C.

The effect of annealing temperature on the average grain size and crystallinity was studied by XRD. Figure 7a illustrates all reflections corresponding to the anatase phase. No other phases are observed. XRD results revealed that the

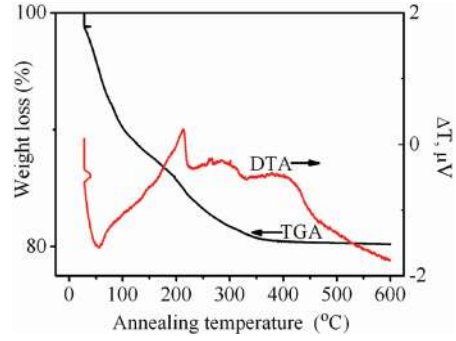

FIGURE 6. TGA/DTA curves for TiO_2 sample annealed at 100 °C.

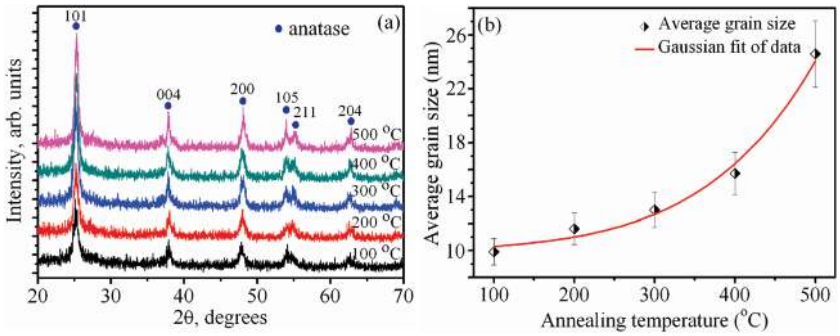

FIGURE 7. (a) XRD patterns of TiO_2 thin films annealed at various temperatures and (b) the average grain size for TiO_2 thin films vs annealing temperature.

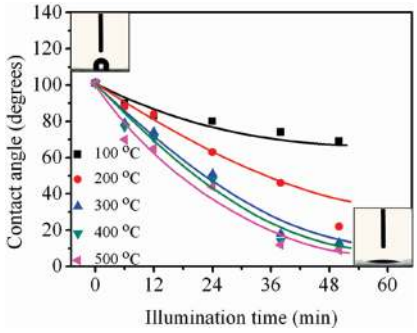

FIGURE 8. Decreasing trend of CA vs UV illumination time (the trend lines are second-order polynomial fits).

intensity of all reflections increased with the annealing temperature. The average grain size was calculated by using Debye–Scherer's formula (47, 64, 65) from the full-width at half maximum (FWHM) of the (101) reflection:

$$D = \frac{0.9\lambda}{[B\cos\theta]}, B = \sqrt{B_m^2 - B_s^2} \qquad (1)$$

where D is the crystallite size or grain size, λ is the X-ray radiation wavelength; B_m and B_s are the reflection FWHM of the measured sample and the standard sample, respectively.

The average grain size presents an increasing trend with annealing temperature, where the major increase occurred after 300 °C. The estimated average grain size ranges from 10 nm to 25 nm for 100 °C to 500 °C annealed samples. Increasing the annealing temperature has evidently enhanced the grain size.

3.4. Photocatalytic activity. Decomposition of stearic acid was used to measure the photocatalytic properties of the films. Figure 8 shows a decreasing trend of CA vs UV illumination time. UV illumination has led to stearic acid decomposition causing CA values reduction. The initial CA of the TiO_2 films (after preparation, they were kept in the dark for 20 h) before and after applying stearic acid was ~10 and ~101°, respectively. One notes that the rate of decomposition (the rate of CA reduction vs illumination time) is higher for higher annealing temperatures; however, no significant improvement was observed after 300 °C.

DISCUSSION

The composition of TiO_2 film changes continuously during processing, from dipping to its final transformation to a solid oxide film after annealing. This has been demonstrated by the XPS results. The nanoparticle sol, which is used for the deposition of films, consists of water, TiO_2 nanoparticles, and a small portion of isopropyl alcohol. As the film is applied, the majority of the water and alcohol in the sol evaporate. This leads to an evaporation-induced condensation reaction, which creates Ti–O–Ti bonds from the unreacted hydrolyzed precursors, as well as between Ti–OH groups on the particles surface. Condensation of Ti–OH groups on the surface provides interconnects between the particles, leading to a solid granular film. Nanoparticle sols created from the peroxotitanium complex have a high concentration of active OH groups on the surface.

It has been demonstrated that materials with nano-sized grains exhibit different mechanical properties, compared to the polycrystalline materials with grain sizes of micrometer size or larger (66–70). Moreover, as observed in this work, the granular morphology is another factor that plays an important role in nanomechanical properties; i.e., the way the material deforms under an external force. The hardness and reduced modulus for TiO_2 films grown by sputtering (which is closer to bulk TiO_2) are reported to be about 8 and 170 GPa, respectively (71). Comparing these values with our results (hardness $\approx$ 1 GPa, $E_r \approx$ 10 GPa), shows the hardness and modulus are considerably smaller than for the granular films. This is a morphology related effect. During the dip-coating process the nanoparticles pile up on the substrate; an evaporation-induced condensation reaction takes place, where nanoparticles bind together from their contact interfaces. This forms a highly porous, granular structure, where the mechanical properties are highly influenced by the relatively weak binding between the particles. It has been reported that granular films show compaction behavior of a loosely packed granular material because neighboring grains slide around and past each other, which results in completely different mechanical properties, compared with non-granular films, such as sputtered films or bulk materials (47, 72).

In this work, we have observed no pile-up at the edges of residual indents or scratches on TiO_2 films, despite the fact that the films show plastic behavior and exhibit negligible recovery. We believe that when these granular films undergo indentation, neighboring grains slide around, pass each other and try to occupy the empty spaces. This definitely cannot happen in dense structures. Figure 9 shows a sche-

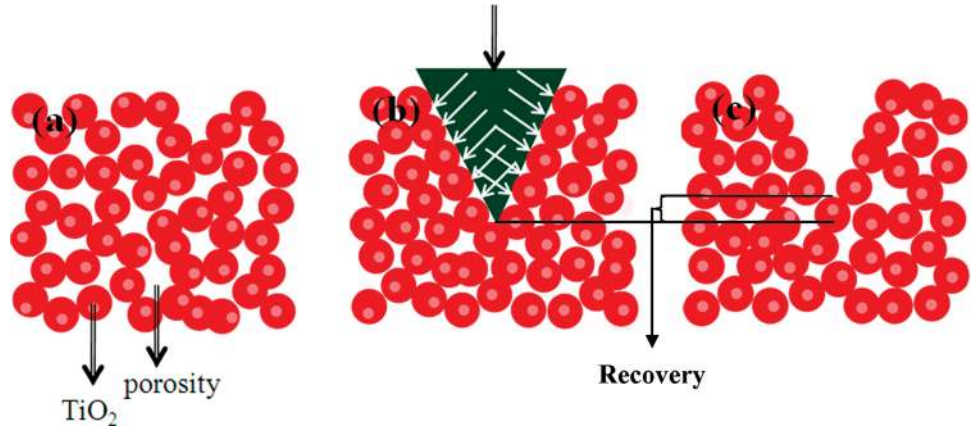

FIGURE 9. Schematic of the molecular ordering in layered TiO_2 oxides, assuming granular and porous TiO_2: (a) before indentation, (b) under indentation load, and (c) after indentation.

matic of nanoparticles ordering in a granular TiO_2 film, illustrating what can happen under indentation. Figure 9a shows TiO_2 film before indentation. Under indentation TiO_2 nanoparticles are compressed into the empty spaces (Figure 9b). This explains why pile-up effect is observed in dense materials, where there is not enough empty space. After indentation, a very small slide recovery happens due to the plastic nature of deformation.

Apart from the considerably lower hardness and modulus for our granular films compared to the bulk values, a main observation in this work is that 300 °C is an optimum annealing temperature in terms of mechanical properties; that is, temperatures greater than 300 °C lead to lower hardness and modulus of elasticity. We discuss two possible sources of this effect: (1) iIncrease in the grain size, (2) diffusion of Na ions into the film from the soda lime glass substrate.

The average grain size can affect the hardness of materials according to a phenomenological Hall−Petch equation (73)

$$H = H_i + KD^{-1/2} \qquad (2)$$

where H_i, D, and K represent the lattice friction stress, the grain size, and the Hall−Petch constant, respectively. Equation 2 implies that increasing the average grain size of a material would cause its hardness to decrease. However, the Hall−Petch equation is a phenomenological relationship based on the motion of dislocations and is typically applied for metals, where plastic deformation is restricted by the grain size. It can hardly be used for ceramics with limited plasticity. In granular materials, plastic deformation can be accommodated by porous film densification, and the Hall−Petch equation cannot be applied.

To verify the possible contribution of the Na ions diffusion from the glass substrate, we deposited identical TiO_2 films on fused silica substrates and carried out nanoindentation tests. It was first confirmed that the morphology and grain size of both films were identical, using AFM images. The hardness values for the films on glass and fused silica substrates are shown in Figure 10. There is a clear deviation for annealing temperatures above 300 °C; that is, the hardness values continue to increase for the films deposited

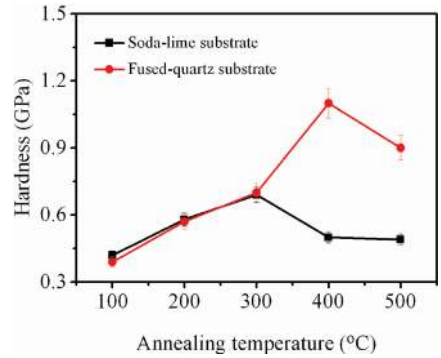

FIGURE 10. Comparison graph for hardness of TiO_2 layers over soda-lime and fused-quartz substrates vs annealing temperature.

on fused silica substrate, whereas they decrease for the films deposited on glass substrate. This evidently demonstrates that the reduction of hardness above 300 °C annealing is an effect related to the substrate. XPS data (Figure 4) confirm that the diffusion of Na starts approximately from 300 °C annealing temperature. Diffusion of Na ions from the glass substrate is a known phenomenon for photocatalyst films on soda lime glass substrates (74, 75).

For a granular film that has a high internal surface area, one expects that the diffusion from the substrate takes place mainly on the surface of grains (particles), that is, the diffusion is dominated by surface diffusion. This suggests that the concentration of the diffused Na ions is highest on the surface of grains and at the interface between the grains. Because the mechanical properties of the granular film are governed by the strength of the bonding between the grains, the inclusion of Na into the material at the neck between the grains may cause remarkable influence on the hardness and elastic modulus.

It is well known in glass industry that inclusion of sodium into silicate glasses results in softer glasses, with lower melting/softening point. In SiO_2−Na_2O glass systems, the introduction of Na ions disrupts the Si−O−Si bonds of the silica glass network according to the eq 3

$$\equiv Si-O-Si \equiv + 2Na^+ \rightarrow \equiv Si-O-Na + Na-O-Si\equiv \qquad (3)$$

where Na is ionically bonded to the oxygen atoms, thus impairing the lattice continuity. In the meantime, Si atoms are connected to O atoms by covalent bonds, whereas the Si−O−Si network is extremely stable because of the strength of these covalent bonds. Introduction of highly mobile Na ions from the substrate leads to a relatively loose network because of formation of ionic bonds which are much weaker than covalent bonds (76, 77).

We believe that a similar effect occurs in our granular TiO_2 films, as Na diffuses from the substrate. The Na ions diffuse mainly on the surface of grain, and affect the necks between the grains by replacing the high strength Ti−O−Ti bonds with weaker Ti−O−Na bonds. The mechanical properties of the TiO_2 granular film are strongly affected by the nature of bonds connecting the neighboring grains. This may explain why Na diffusion reduces the hardness and modulus.

It is generally believed that Na ions diffusion from the substrates into TiO_2 films has an adverse effect on photocatalytic properties. This has been associated with the prevention or decrease in photoactive anatase phase formation as a consequence of high Na concentration or formation of Na_xTiO_2 phase near the film surface, enhancing the recombination of photogenerated electrons and holes (74, 75). There are also opposing reports that have shown that Na enhances the anatase crystal formation (33). We observe that the photocatalytic activity is enhanced with heat treatment temperature up to 300 °C (Figure 8). This should be attributed to the removal of the volatile phase out of the film, resulting in a more pure and crystalline TiO_2 phase in the films. There is some amorphous phase in the as-deposited films, which turns into crystalline phase due to heat treatment, leading to improved photocatalytic activity. The trend of crystallization continues after 300 °C annealing with a more rapid pace (Figure 7). More crystalline material implies lower concentration of defects, hence lower recombination rate and higher photocatalytic activity. Nevertheless, not much enhancement in photocatalytic activity was observed past 300 °C annealing (Figure 8). This might be due to the simultaneous occurrence of sodium diffusion from the substrate after 300 °C annealing, which compensates the positive effect of crystallization, resulting in a more or less saturated photocatalytic activity for heat treatments above 300 °C.

4. CONCLUSIONS

It was observed that granular films of TiO_2 deposited on soda-lime glass substrates exhibit optimal mechanical properties for heat treatment temperature of 300 °C. Contrary to what was expected, increasing the heat treatment temperature above 300 °C results in lower values of hardness and modulus of elasticity. The values are, however, an order of magnitude smaller than the bulk values, demonstrating that the granular/porous morphology plays the dominant role in mechanical properties. The granular structure also leads to the absence of pile-up effect, which is typically observed in indentation. XPS and TG/DTA data show that the composition of the film continuously changes with the heat treatment temperature. For the annealing temperatures below 300 °C, the dominant phenomena are the removal of water from the film and an evaporation-induced condensation and densification of the films. Above 300 °C, the main trend is the increase in Na concentration with temperature because of Na diffusion from the soda lime glass substrate.

Heat treatment also improves the crystallinity of TiO_2. This is in particular notable for temperatures above 300 °C, as evidenced by XRD data. Nevertheless, this improved crystallinity for heat treatments above 300 °C, has not led to an improved photocatalytic activity, possibly because of the adverse effect of Na diffusion from the substrate into the film, mainly above 300 °C. We believe that the deterioration of the mechanical properties for heat treatments above 300 °C is also a result of sodium inclusion into the film. This may result in low strength Ti−O−Na−O−Ti bonds at the neck between the grains that considerably reduces the hardness and elastic modulus of the granular films.

This finding that 300 °C is an optimal heat treatment temperature for granular TiO_2 films deposited on glass substrate, is of practical importance, as 300 °C is achievable using heat guns or other low cost techniques; hence it can be used for the on-site applications, where coatings cannot be applied in a factory.

Supporting Information Available: Table of nanomechanical properties, AFM images and load−displacement curves, evidence for the absence of pile-up and sink-in effects, XPS data for all temperatures, the data on scratch resistance, Hall−Petch plot for TiO_2/glass (hardness as a function of $1/D^{0.5}$), and the surface morphology of TiO_2 thin film annealed at 500 °C over fused quartz and soda-lime glass substrates (PDF). This material is available free of charge via the Internet at http://pubs.acs.org.

REFERENCES AND NOTES

(1) Fujishima, A.; Zhang, X.; Tryk, D. A. *Surf. Sci. Rep.* **2008**, *63*, 515–582.
(2) Kemmitt, T.; Al-Salim, N. I.; Waterland, M.; Kennedy, V. J.; Markwitz, A. *Curr. Appl Phys.* **2004**, *4*, 189–192.
(3) Fujishima, A.; Hashimoto, K.; Watanabe, T. *TiO2 Photocatalysis: Fundamentals and Applications*; BKC: Tokyo, 1999.
(4) Hashimoto, K.; Irie, H.; Fujishima, A. *J. Appl. Phys.* **2005**, *44*, 8269–8285, Japan.
(5) Fujishima, A.; Zhang, X. *C. R. Chim.* **2006**, *9*, 750–760.
(6) Baek, W. H.; Seo, II.; Yoon, T. S.; Lee, H. H.; Yun, C. M.; Kim, Y. S. *Sol. Energy Mater. Sol. Cells* **2009**, *93*, 1587–1591.
(7) Lee, K. M.; Suryanarayanan, V.; Ho, K. C. *Sol. Energy Mater. Sol. Cells* **2007**, *91*, 1416–1420.
(8) Grätzel, M. *Nature* **2003**, *421*, 586–587.
(9) Bach, U.; Lupo, D.; Comte, P.; Moser, J. E.; Weissortel, F.; Salbeck, J.; Spreitzer, H.; Gratzel, M. *Nature* **1998**, *395*, 583–585.
(10) Huang, S. Y.; Schlichthorl, G.; Nozik, A. J.; Gratzel, M.; Frank, A. J. *J. Phys. Chem. B* **1997**, *101* (14), 2576–2582.
(11) Hendry, E.; Wang, F.; Shan, J.; Heinz, T.F.; Bonn, M. *Phys. Rev. B* **2004**, *69*, 081101-4.
(12) Zhang, X. T.; Sato, O.; Taguchi, M.; Einaga, Y.; Murakami, T.; Fujishima, A. *Chem. Mater.* **2005**, *17*, 696–700.
(13) Zhang, X.; Fujishima, A.; Jin, M.; Emeline, A. V.; Murakami, T. *J. Phys. Chem. B* **2006**, *110*, 25142–25148.
(14) Ghadiri, E.; Taghavinia, N.; Zakeeruddin, S. M.; Gratzel, M.; Moser, J.-E. *Nano Lett.* **2010**, *10* (5), 1632–1638.
(15) Zhang, L.; Kanki, T.; Sano, N.; Toyoda, A. *Sep. Purif. Technol.* **2003**, *31*, 105–110.
(16) Cermenati, L.; Pichat, P.; Guillard, C.; Albini, A. *J. Phys. Chem. B* **1997**, *101* (14), 2650–2658.

(17) Rincón, A.-G.; Pulgarin, C. *Appl. Catal., B: Environ.* **2004**, *51*, 283–302.
(18) Fernández, P.; Blanco, J.; Sichel, C.; Malato, S. *Catal. Today* **2005**, *101*, 345–352.
(19) Duffy, E. F.; Al Touati, F.; Kehoe, S. C.; McLoughlin, O. A.; Gill, L. W.; Gernjak, W.; Oller, I.; Maldonado, M. I.; Malato, S.; Cassidy, J.; Reed, R. H.; McGuigan, K. G. *Solar Energy* **2004**, *77*, 649–655.
(20) Taranto, J.; Frochot, D.; Pichat, P. *Ind. Eng. Chem. Res.* **2009**, *48* (13), 6229–6236.
(21) Jo, W.-K.; Park, K.-H. *Chemosphere* **2004**, *57*, 555–565.
(22) Pichat, P.; Disdier, J.; Hoang-Van, C.; Mas, D.; Goutailler, G.; Gaysse, C. *Catal. Today* **2000**, *63*, 363–369.
(23) Ao, C. H.; Lee, S. C. *Appl. Catal., B: Environ.* **2003**, *44*, 191–205.
(24) Chawengkijwanich, C.; Hayata, Y. *Int. J. Food Microbiol.* **2008**, *123*, 288–292.
(25) Maneerat, C.; Hayata, Y. *Int. J. Food Microbiol.* **2006**, *107*, 99–103.
(26) Fujishima, A.; Honda, K. *Nature* **1972**, *37*, 238–245.
(27) Tada, H.; Tanaka, M. *Langmuir* **1997**, *13*, 360–364.
(28) Negishi, N.; Iyoda, T.; Hashimoto, K.; Fujishima, A. *Chem. Lett.* **1995**, 841–842.
(29) Asahi, R.; Morikawa, T.; Ohwaki, T.; Aoki, K.; Taga, Y. *Science* **2001**, *293*, 269–271.
(30) Maeda, M.; Watanabe, T. *J. Electrochem. Soc.* **2006**, *153*, 186–189.
(31) Diwald, O.; Thompson, T. L.; Zubkov, T.; Goralski, E. G.; Walck, S. D.; Yates, J. T. *J. Phys. Chem. B* **2004**, *108*, 6004–6008.
(32) Sakthivel, S.; Kisch, H. *Chem. Phys. Chem.* **2003**, *4*, 487–490.
(33) Nam, H.-J.; Amemiya, T.; Murabayashi, M.; Itoh, K. *J. Phys. Chem. B* **2004**, *108*, 8254–8259.
(34) Breuils, J.; Pelletier, H.; Krier, J.; Vignal, V. *Surf. Coat. Technol.* **2010**, *204*, 2068–2072.
(35) Rodriguez, J.; Rico, A.; Otero, E.; Rainforth, W. M. *Acta Mater.* **2009**, *57*, 3148–3156.
(36) Beegan, D.; Chowdhury, S.; Laugier, M.T. *Thin Solid Films* **2004**, *466*, 167–174.
(37) Chen, J.; Bull, S. J. *Surf. Coat. Technol.* **2009**, *203*, 1609–1617.
(38) Shen, Y. F.; Xue, W. Y.; Wang, Y. D.; Liu, Z. Y.; Zuo, L. *Surf. Coat. Technol.* **2008**, *202*, 5140–5145.
(39) Li, M.; Palacio, M. L.; Carter, C. B.; Gerberich, W. W. *Thin Solid Films* **2002**, *416*, 174–183.
(40) Palacio, M. L.; Wang, Y.; Gerberich, W. W. *J. Mater. Res.* **2001**, *16*, 3628–3635.
(41) Shi, X.L.; Yang, H.; Shao, G.; Duan, X.; Xiong, Z. *Mater. Charact.* **2008**, *59*, 374–379.
(42) Cheng, Y. T.; Cheng, C. M. *Mater. Sci. Eng., R* **2004**, *44*, 91–149.
(43) Dao, M.; Chollacoop, N.; Van Vliet, K. J.; Venkatesh, T. A.; Suresh, S. *Acta Mater.* **2001**, *49*, 3899–3918.
(44) Venkatesh, T. A.; Van Vliet, K. J.; Giannakopoulos, A. E.; Suresh, S. *Scr. Mater.* **2000**, *42*, 833–839.
(45) Volinsky, A. A.; Gerberich, W. W. *Microelectron. Eng.* **2003**, *69*, 519–527.
(46) Volinsky, A. A.; Moody, N. R.; Gerberich, W. W. *Acta Mater.* **2002**, *50*, 441–466.
(47) Yaghoubi, H.; Taghavinia, N.; Keshavarz Alamdari, E. *Surf. Coat. Technol.* **2010**, *204*, 1562–1568.
(48) Taghavinia, N.; Yao, T. *Physica E* **2004**, *21*, 96–102.
(49) MacLeod, H. A. *Thin-Film Optical Filters*, 3rd ed.; Taylor & Francis: London, 2001.
(50) Heavens, O. S. *Optical Properties of Thin Solid Films*; Dover Publications: Mineola, NY, 1965.
(51) Bhushan, X.; Li, B. *Mater. Charact.* **2002**, *48*, 11–36.
(52) Bhushan, B.; Li, X. *Int. Mater. Rev.* **2003**, *48*, 125–164.
(53) Hosseini, Z.; Taghavinia, N.; Sharifi, N.; Chavoshi, M.; Rahman, M. *J. Phys. Chem. C* **2008**, *112*, 18686–18689.
(54) Oliver, W. C.; Pharr, G. M. *J. Mater. Res.* **1992**, *7*, 1564–1580.
(55) Barry Carter, C.; Grant Norton, M. *Ceramic Materials Science and Engineering*; Springer: New York, 2007.
(56) Pharr, G. M. *Mater. Sci. Eng., A* **1998**, *253* (1−2), 151–159.
(57) Henderson, M. A. *Langmuir* **1996**, *12*, 5093–5098.
(58) Wang, R.; Sakai, N.; Fujishima, A.; Watanabe, T.; Hashimoto, K. *J. Phys. Chem. B* **1999**, *103* (12), 2188–2194.
(59) Wang, R.; Hashimoto, K.; Fujishima, A.; Chikumi, M.; Kojima, E.; Kitamura, A.; Shimohigoshi, M.; Watanabe, T. *Adv. Mater.* **1998**, *10*, 135–138.
(60) Lu, G.; Linsebigler, A.; Yates, J. T. *J. Phys. Chem.* **1994**, *98* (45), 11733–11738.
(61) Zhu, J.; Yang, J.; Bian, Z. F.; Ren, J.; Liu, Y. M.; Cao, Y.; Li, H. X.; He, H. Y.; Fan, K. N. *Appl. Catal., B* **2007**, *76*, 82–91.
(62) Guillard, C.; Debayle, D.; Gagnaire, A.; Jaffrezic, H.; Herrmann, J. M. *Mater. Res. Bull.* **2004**, *39*, 1445–1458.
(63) Egashira, M.; Kawasumi, S.; Kagawa, S.; Seiyama, T. *Bull. Chem. Soc. Jpn.* **1978**, *51*, 3144–3149.
(64) Cullity, B. D. *Elements of X-Ray Diffraction*, 2nd ed.; Addison-Wesley: Reading, MA, 1978.
(65) Bilik, P.; Plesch, G. *Scr. Mater.* **2007**, *56*, 979–982.
(66) Schiøtz, J.; Di Tolla, F. D.; Jacobsen, K. W. *Nature* **1998**, *391*, 561–563.
(67) Yip, S. *Nature* **1998**, *391*, 532–533.
(68) Szlufarska, I. *Mater. Today* **2006**, *9* (5), 42–50.
(69) Liao, F.; Girshick, S. L.; Mook, W. M.; Gerberich, W. W.; Zachariah, M. R. *Appl. Phys. Lett.* **2005**, *86*, 171913.
(70) Chen, D.; Zhang, X.-F.; Ritchie, R. O. *J. Am. Ceram. Soc.* **2000**, *83*, 2079–2081.
(71) Zywitzki, O.; Modes, T.; Sahm, H.; Frach, P.; Goedicke, K.; Glöss, D. *Surf. Coat. Technol.* **2004**, *180−181*, 538–543.
(72) Lee, D.; Jia, S.; Banerjee, S.; Bevk, J.; Herman, I. P.; Kysar, J. W. *Phys. Rev. Lett.* **2007**, *98*, 026103.
(73) Venkatraman, R.; Bravman, J. C. *J. Mater. Res.* **1992**, *7*, 2040–2048.
(74) Paz, Y.; Heller, A. *J. Mater. Res.* **1997**, *12*, 2759–2766.
(75) Paz, Y.; Luo, Z.; Rabenberg, L.; Heller, A. *J. Mater. Res.* **1995**, *10*, 2842–2848.
(76) Mehrer, H.; Imre, A. W.; Tanguep-Nijokep, E. *J. Phys.: Conf. Ser.* **2008**, *106*, 012001.
(77) Shelby, J. E. *Introduction to Glass Science and Technology*; The Royal Society of Chemistry: London, 1997.

AM100455Q

Supporting Information Available

Nanomechanical properties of TiO_2 granular thin films

Ms. Ref. No.: am-2010-00455q

Houman Yaghoubi[1], *Nima Taghavinia*[2, 3]*, *Eskandar Keshavarz Alamdari*[1, 4], *Alex A. Volinsky*[5]

[1] New Materials Department, Materials and Energy Research Center (MERC), P.O. Box 14155-4777, Tehran, Iran

[2] Physics Department, Sharif University of Technology, Tehran 14588, Iran

[3] Institute for Nanoscience and Nanotechnology, Sharif University of Technology, Tehran 14588, Iran

[4] Department of Mining and Metallurgical Engineering, Amirkabir University of Technology, 424 Hafez Avenue, P.O. Box 15875-4413, Tehran, Iran

[5] Department of Mechanical Engineering, University of South Florida, Tampa, FL 33620, USA

*Corresponding author: Fax: +98-(21)-66164532, E-mail: taghavinia@sharif.edu

E-mail addresses: Yaghoubi.houman@gmail.com (H. Yaghoubi), Taghavinia@sharif.edu (N. Taghavinia), alamdari@aut.ac.ir (E. K. Alamdari), volinsky@usf.edu (A. A. Volinsky)

Table S1. Numerical data for nanoindentation tests of TiO_2 layers on glass annealed between 100 °C and 500 °C.

Temp. (°C)	Load (μN)	Max. Force (μN)	Max. Depth h_{max} (nm)	Contact Depth (nm)	Contact Stiffness (μN/nm)	H (GPa)	E_r (GPa)	Contact Area (nm^2)	Power-law coefficients $P=A(h-h_f)^m$		
									A	h_f	M
100	125	112.5	78.2	73.3	38.0	0.42	9.5	2.672E+5	4.048	69.82	1.915
200	125	114.0	66.0	61.0	35.1	0.58	10.3	1.955E+5	2.477	56.89	2.031
300	125	114.8	60.9	56.8	34.1	0.69	10.6	1.731E+5	3.835	53.06	1.855
400	125	113.2	71.1	66.9	35.7	0.50	9.7	2.283E+5	4.176	63.36	1.860
500	125	114.1	73.1	68.8	33.2	0.49	9.6	2.396E+5	3.528	64.93	1.869

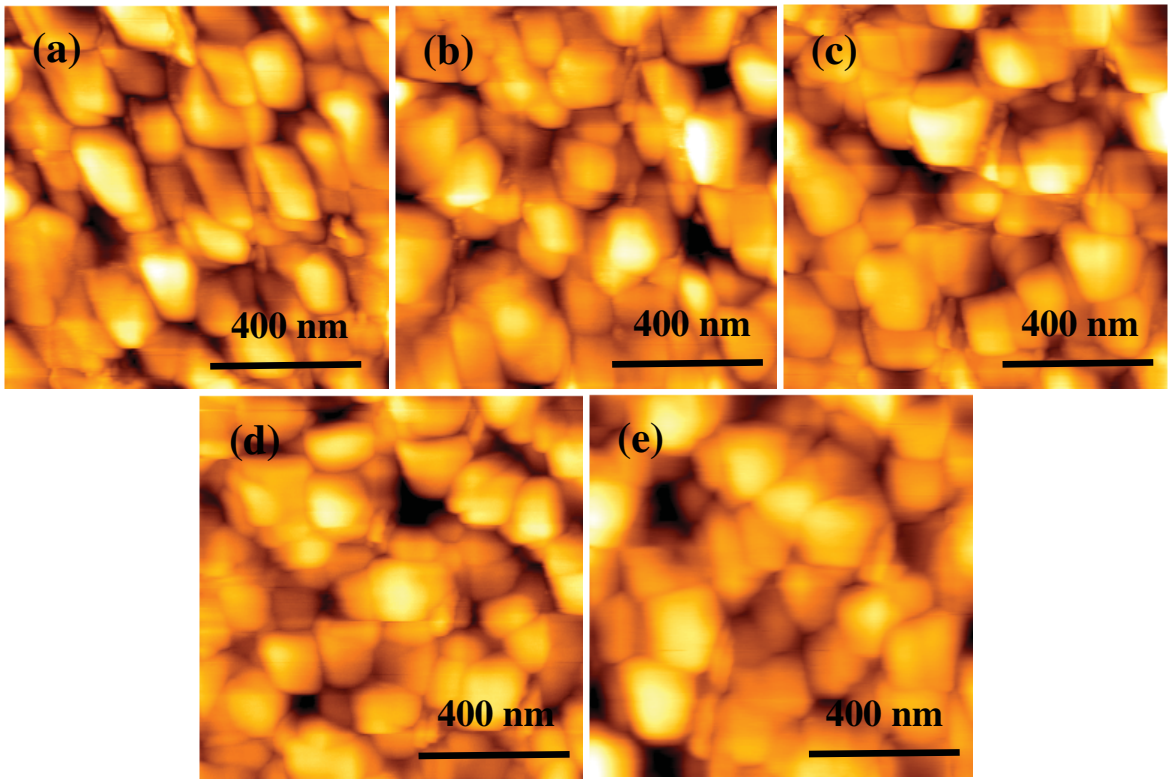

Figure S1. Surface morphology of TiO_2 films annealed at: (a) 100 °C, (b) 200 °C, (c) 300 °C, (d) 400 °C and (e) 500 °C.

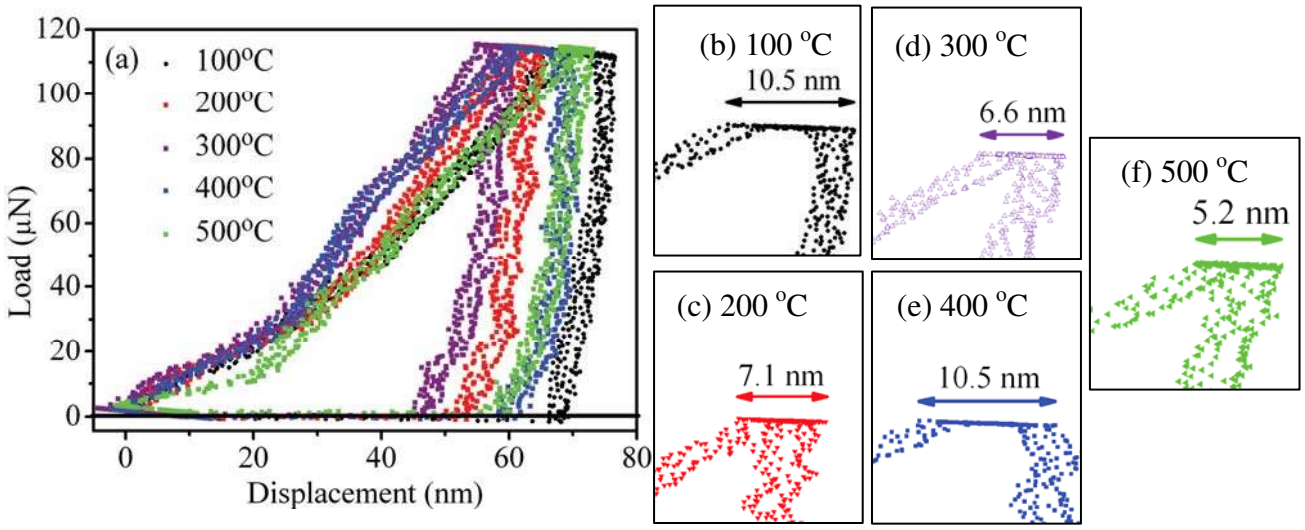

Figure S2. (a) Typical load-displacement curves for the TiO_2 films annealed between 100 °C and 500 °C; (b-f) displacement during hold time (creep) for films annealed between 100 °C and 500 °C.

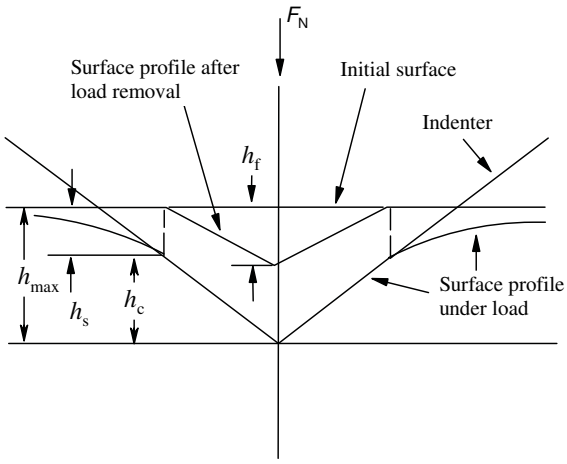

Figure S3. Assumed contact geometry with definition of h_{max} under load and h_f as the final depth of the impression after unloading (contact geometry under load and after unloading).

Figure S3 provides a better view of the mentioned parameters and depicts assumed contact geometry under load and after unloading.

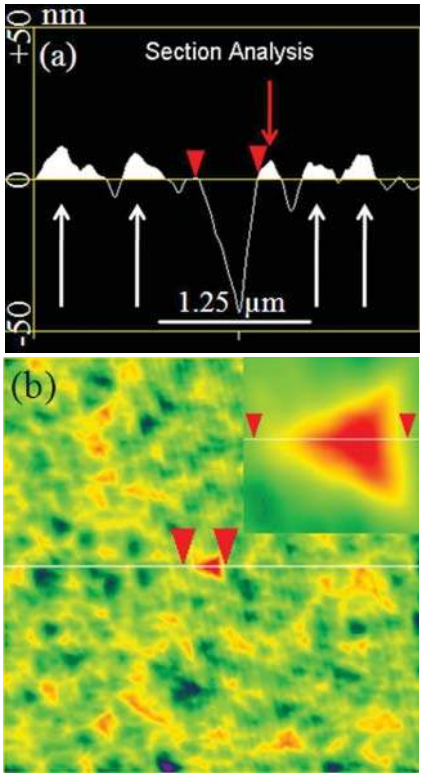

Figure S4. (a) Section analysis and (b) corresponding AFM image of the 125 µN indent of the TiO_2 film annealed at 100 ^oC.

AFM images and the corresponding section analysis plots of a 125 µN indent on the 100 ^{o}C annealed sample are presented in Figure S4 (a, b). Figure S4 clearly shows that there is no pile-up or sink-in at the edges of the residual indent. This statement is also true for the films annealed between 200 ^{o}C and 500 ^{o}C. White hump seen at the right edge of residual indent in Figure S4a is the roughness artifacts and should not be regarded as the pile-up effect, since similar humps are present in portions of the section profile far from the indent. The average height of these humps is about 12 nm, similar to AFM topographical images.

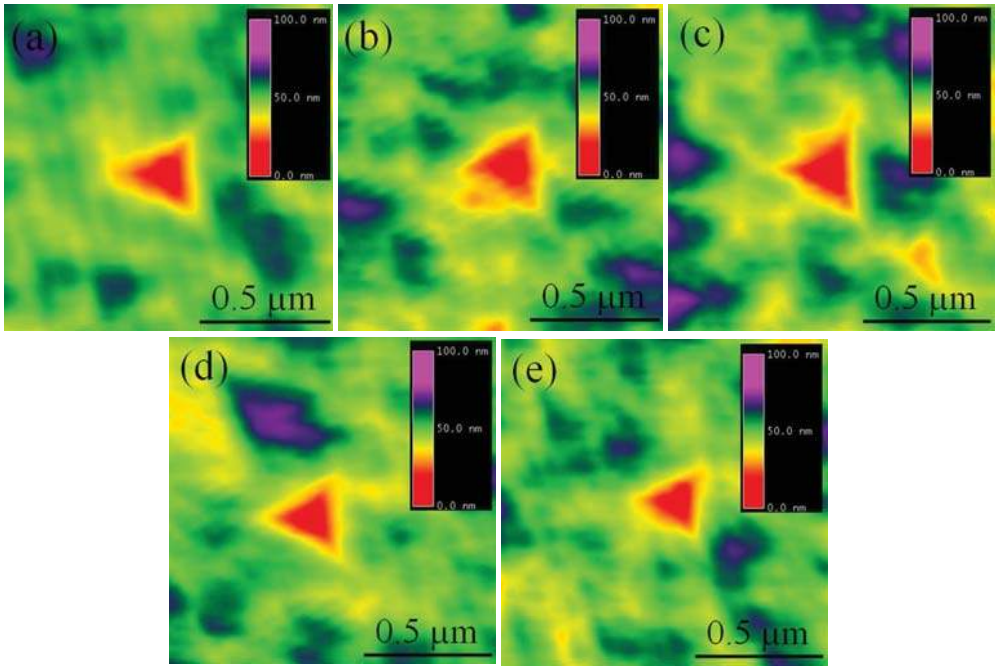

Figure S5. Selection of AFM images of the residual indents on the TiO_2 films annealed at (a) 100 ^{o}C, (b) 200 ^{o}C, (c) 300 ^{o}C, (d) 400 ^{o}C and (e) 500 ^{o}C.

To obtain a precise picture of what is really happening under indentation residual indentations were imaged for better quantification of nanoindentation results, i.e. pile up and/or sink-in effects and elastic/plastic behavior. Figure S5 shows AFM images of select 125 µN residual indents in TiO_2 films annealed between 100 ^{o}C and 500 ^{o}C. Indentation images evidently confirm plastic nature of the TiO_2 films' deformation and/or contact.

Images in Figure S5 correspond to load-displacement curves in the paper (Figure. 2). Moreover, no pile up and sink-in effects are observed.

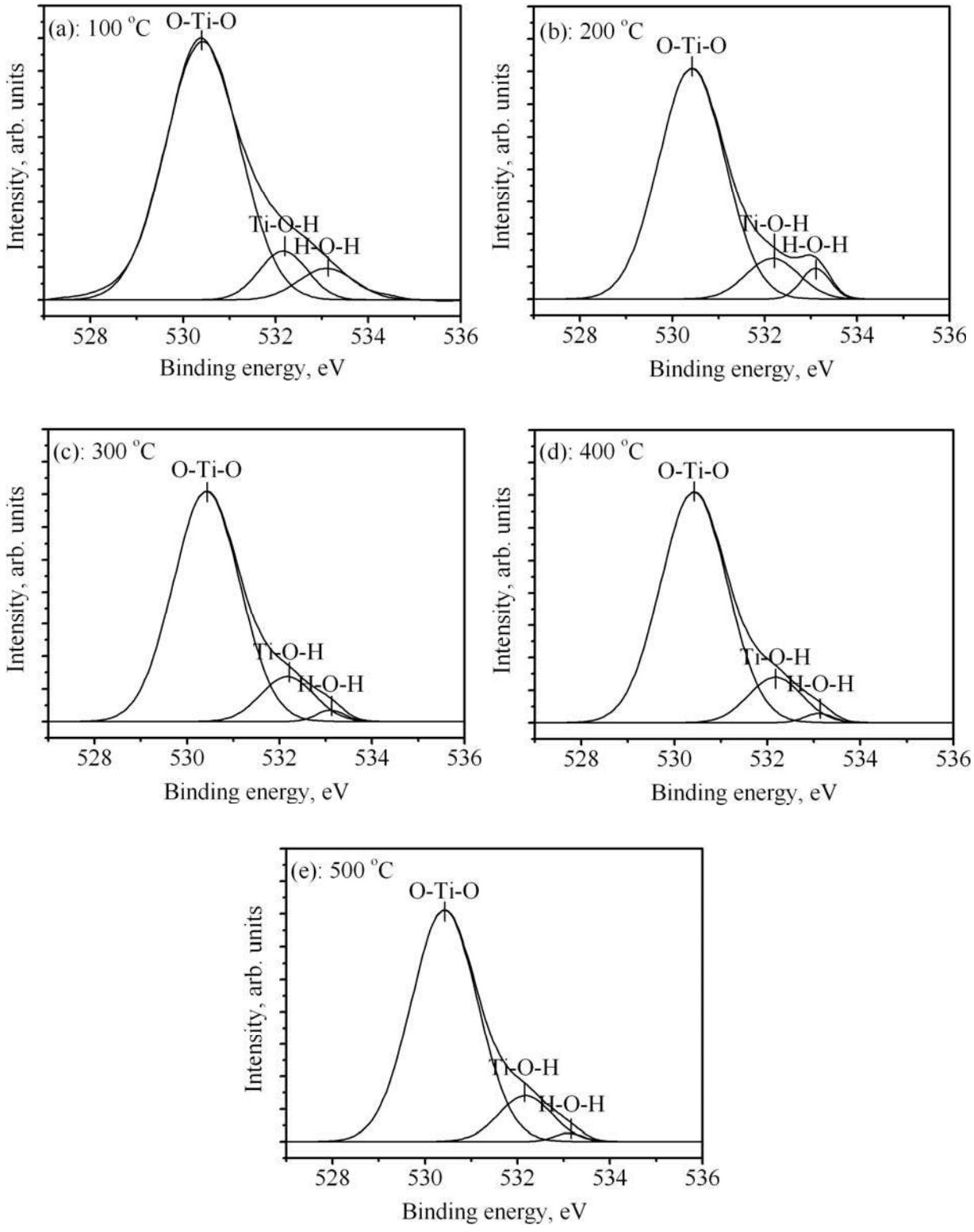

Figure S6. (a-e) XPS spectra of the O 1s region for the samples annealed between 100 °C and 500 °C.

In order to determine film scratch resistance at constant normal force, three approaches have been undertaken based on: 1. The volume of the excavated ditch (the scratch

volume) [47] or the scratch area, 2. The scratch depth [78] and 3. The friction coefficient along the scratch length [79]. The volume of the excavated ditch and the scratch area can be measured using the AFM images with the section analysis. Residual depth measurements can be performed from a transverse profile section of a nanoscratch groove. The friction coefficient as a measure of the resistance to abrasion is calculated as the ratio of the lateral force over the normal force along the whole scratch length.

Nanoscratch experiments were performed at constant normal force and produced 4 µm scratches. Figure S7 (a) shows the 3D AFM image of the residual scratch on the 100 ^{o}C annealed sample. The volume and the depth of excavated trenches were measured as a function of annealing temperature. The results clearly show decreasing trend of the volume and the depth of scratches with increasing annealing temperature (Figure S7 (b)). The volume of excavated trenches for layers annealed between 100 ^{o}C and 500 ^{o}C was 2.31×10^{-2} µm^3, 2.03×10^{-2} µm^3, 1.2×10^{-2} µm^3, 1.03×10^{-2} µm^3 and 0.97×10^{-2} µm^3, respectively. Moreover, the maximum scratch depth reached 31.6 nm for 100 ^{o}C annealed sample, and only 18.7 nm for 500 ^{o}C, while no significant improvement was observed after 300 ^{o}C annealing. Variation of the friction coefficient vs. temperature along the scratch length was evaluated for all samples (Figure S9). Based on these results, the variation was not reproducible or ordered.

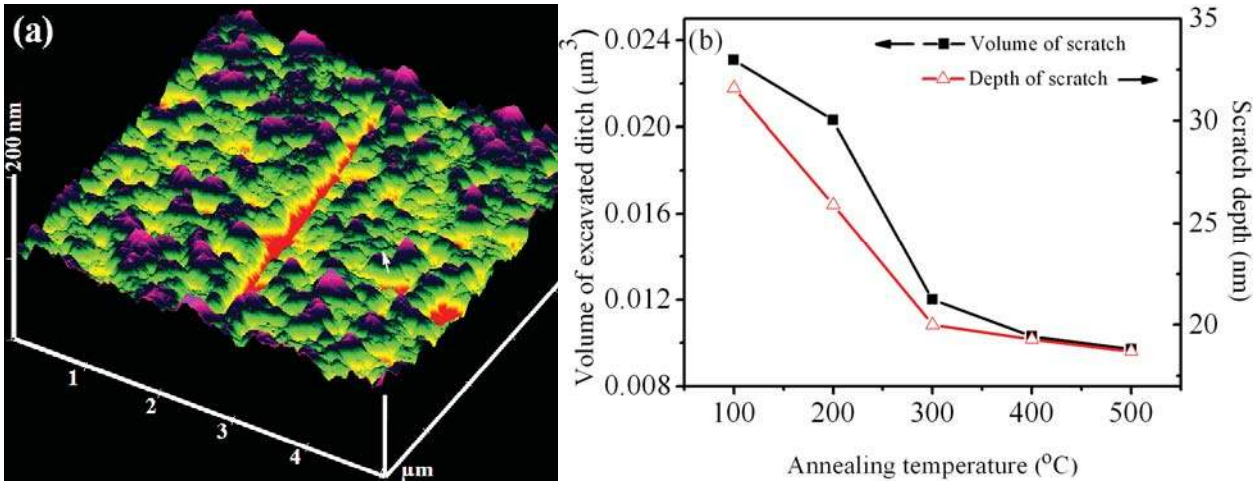

Figure S7. (a) 3D AFM image of the residual scratch on 100 ^{o}C annealed layer, (b) variation of the excavated trench volume and the scratch depth vs. annealing temperature.

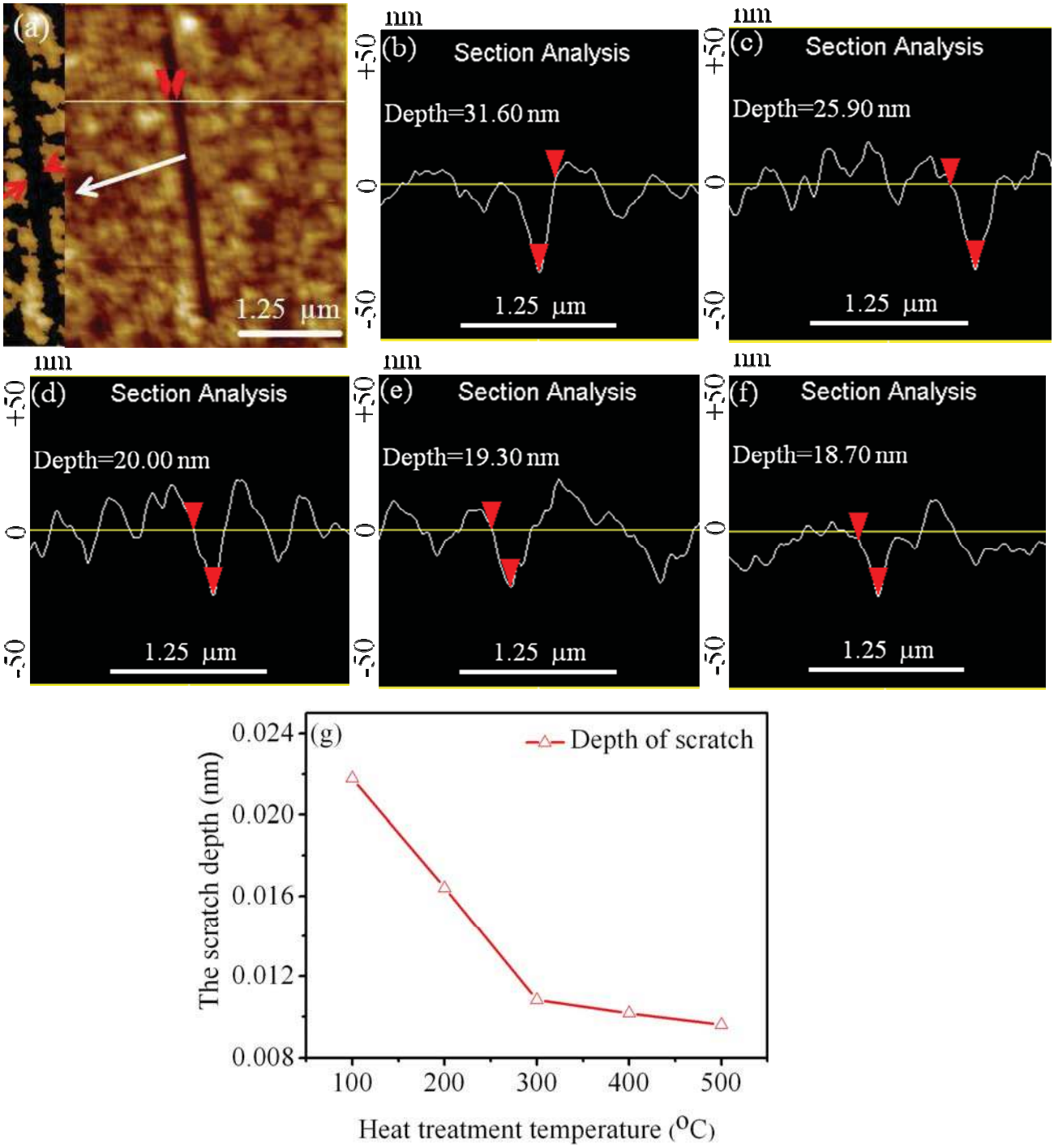

Figure S8. (a) 2D AFM images of a nanoscratch on 100 °C annealed sample; residual depth measurements from transverse section profiles of nanoscratch grooves for (b) 100 °C, (c) 200 °C, (d) 300 °C, (e) 400 °C and (f) 500 °C annealed samples and (g) variation of the scratch depth vs. annealing temperature.

Figure S8 shows a scratch track appearance for the TiO_2 film annealed at 100 °C and section profiles of nanoscratch grooves for samples annealed between 100 °C and 500 °C. Figure S8 (f) clearly displays a shallow wear (scratch) track surface (residual depth of scratch

groove is ~ 18.7 nm), whereas Figure S8 (b) shows a deeper wear (scratch) track surface (residual depth of scratch groove is ~ 31.6 nm). Please note that Figure S8 (g) demonstrates no significant improvement observed after 300 ^{o}C annealing with respect to the scratch resistance.

Figure S8 (a) shows no pile-up effects at the edges of residual nanoscratch imprint, and section analyses also confirm this statement. The humps which occasionally can be seen at the edges of residual scratches are observable at different parts along the scratch length and actually are the roughness artifacts and are not attributed to the pile-up effect.

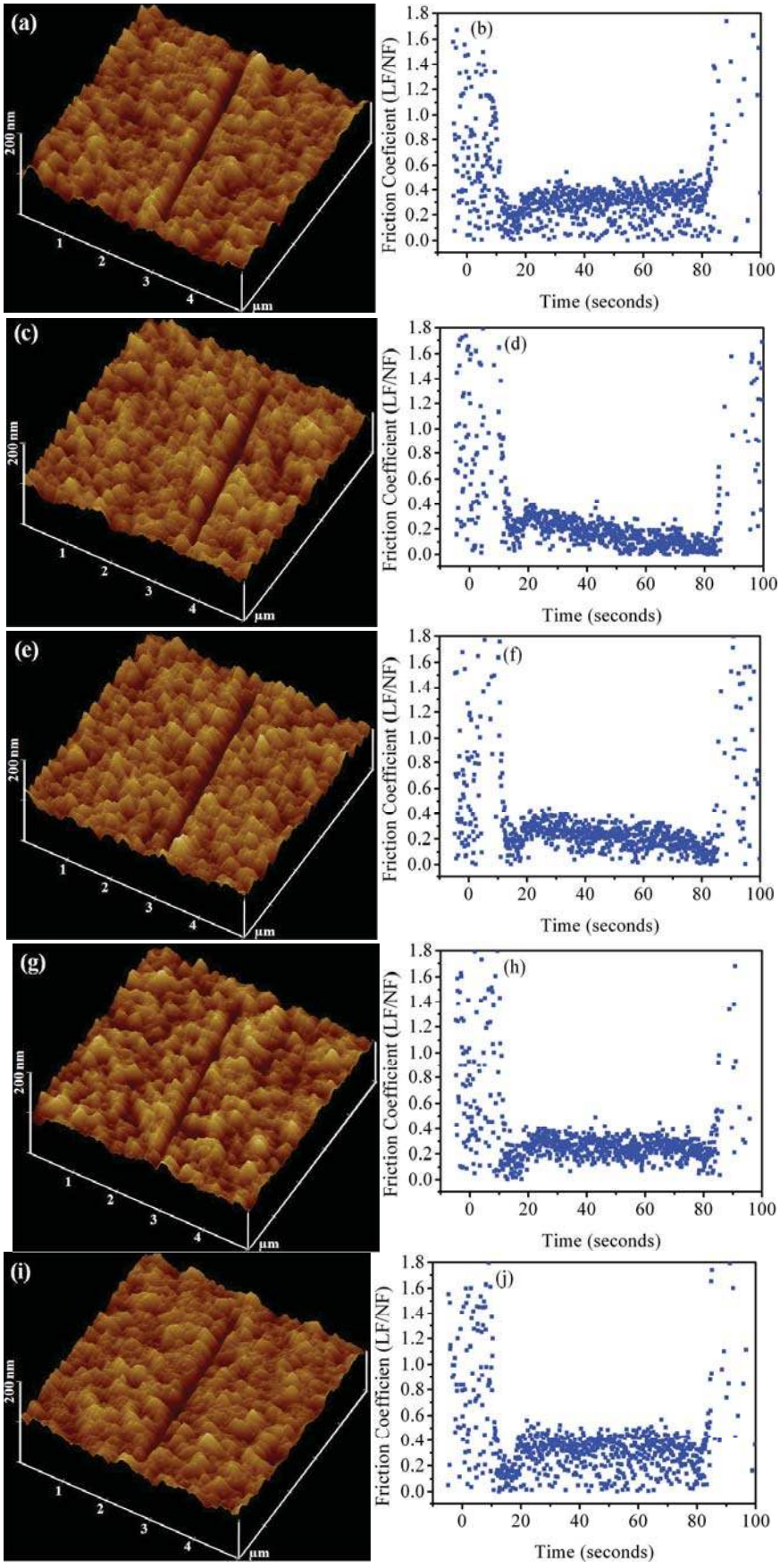
(a)
200 nm
1
2
3
4
µm
(b)
Friction Coefficient (LF/NF)
Time (seconds)
(c)
(d)
(e)
(f)
(g)
(h)
(i)
(j)
Friction Coefficien (LF/NF)

Figure S9. AFM images of residual scratches and variation of the friction coefficient vs. time for layers annealed at (a) 100 °C, (b) 200 °C, (c) 300 °C, (d) 400 °C, (e) 500 °C.

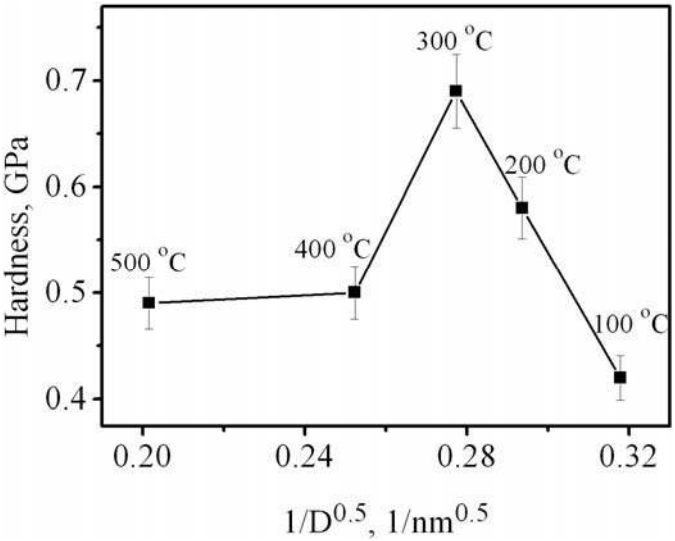

Figure S10. Hall-Petch plot for TiO_2/Glass (hardness as a function of $1/D^{0.5}$).

In order to verify the validity of Hall-Petch equation, the measured hardness values for samples heat treated between 100 °C and 500 °C, were plotted against $D^{-0.5}$ (Figure S10), where D is the grain size estimated from the XRD peak broadening (as indicated in Figure 7). The first data point with the lowest $D^{-0.5}$ value corresponds to 500 °C, and the last one corresponds to 100 °C annealing. The increase in hardness from 100 °C to 300 °C annealed films (the last 3 points) is due to the removal of water from the film, leading to condensation reactions that provide stronger binding of neighboring particles. The decrease in hardness for 300 °C to 500 °C annealed films (the first 3 points) is in direction of Hall-Petch prediction, however, it does not show a linear dependence, that is, the Hall-Petch equation cannot explain the decrease in hardness and modulus after 300 °C annealing temperature.

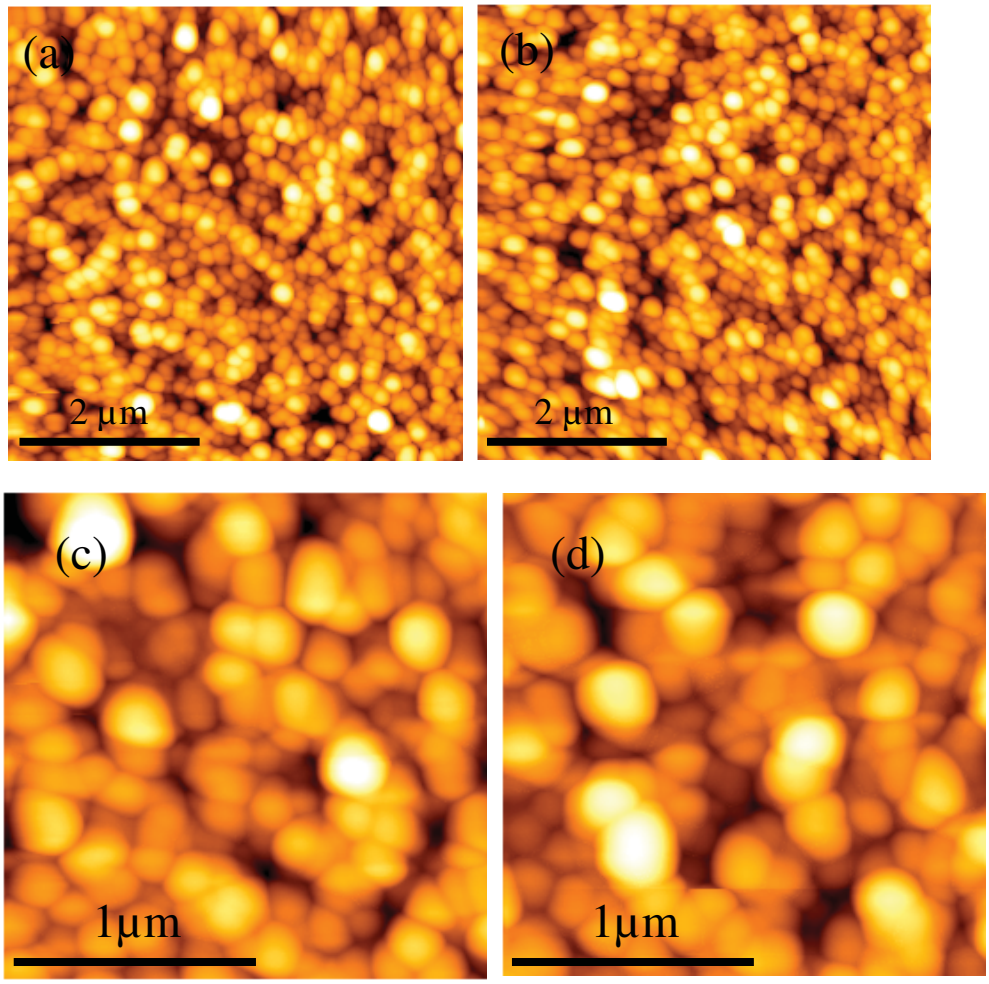

Figure S11. The surface morphology of TiO_2 thin film, for 5 µm windows, annealed at 500 ^{o}C over FQ (a) and SLG (b); for 2 µm windows, annealed at 500 ^{o}C over FQ (c) and SLG (d).

We had observed that the grain size of the film is not much affected by the presence of Na in glass. The AFM images in Figure S11 (a, b for 5 µm window and c, d for 2µm window) show the morphology of films on fused quartz and soda lime glass annealed at 500°C. The average grain sizes are the same within less than about 5%. This supports our conclusion that Na affects the contact of grains rather than the morphology.

This information is available free of charge via the Internet at http://pubs.acs.org.